PHYSICAL REVIEW E VOLUME 58, NUMBER 4 OCTOBER 1998

Three-dimensional simulations of Ostwald ripening with elastic effects

Celeste Sagui,[1] Daniel Orlikowski,[1] Andrés M. Somoza,[2] and Christopher Roland[1]
[1]*Department of Physics, North Carolina State University, Raleigh, North Carolina 27695*
[2]*Departamento de Fisica, Universidad de Murcia, Apartado Postal 4021, E-30080 Murcia, Spain*
(Received 7 April 1998)

The process of phase separation for quenched, *three-dimensional* binary alloy systems with coupled elastic fields was investigated with Langevin simulations. The elastic effects are the result of a dilational misfit introduced via inhomogeneities in the elastic constants of the system. A selection criterion for the shape and/or orientation of the domains, based on the different shear moduli, is presented. In addition, the coarsening behavior of the domains is discussed in terms of chemical potential barriers surrounding the precipitates. [S1063-651X(98)50710-6]

PACS number(s): 64.60.Qb, 05.70.Fh, 64.75.+g, 81.30.Mh

Ostwald ripening refers to the late-stage process by which a minority phase coarsens in a binary alloy mixture. In order to maintain local equilibrium, material from the smaller, high-curvature droplets evaporates and diffuses through the matrix. It then condenses onto nearby larger, low-curvature droplets, thereby lowering the interfacial free energy of the system. This mechanism was described by Lifshitz, Slyozov, and Wagner (LSW) [1] in the limit of zero volume fraction, and exhibits several ''universal'' features. Growth is typically characterized by a single, time-dependent length scale $R(t)$, the average domain size, to which spatial quantities, such as the dynamic structure factor and correlation functions, scale. Furthermore, the average domain size grows with a power law in time with an exponent of 1/3, while the droplet distribution function displays a characteristic scaling behavior.

The process of Ostwald ripening is radically altered in the presence of elastic fields. Generally, it is known that long-range elastic fields destroy the universal features of LSW growth, thereby allowing the system to explore other kinetic alternatives [2]. For instance, many experiments show the formation of modulated structures with a quasiperiodic spatial distribution [2–8]. In binary alloy systems, elastic effects are derived from a lattice mismatch between the different atomic species, from differences in elastic constants of the phases, and/or from externally imposed stresses.

In this Rapid Communication, we report on large-scale, three-dimensional (3D) simulations of Ostwald ripening in the presence of elastic fields for a *cubic, elastically inhomogeneous* system with dilational misfit. The effect of these fields on the formation and growth of droplets, the elastic barriers, and the spatial ordering of domains are discussed. In addition, a selection criterion, predicting both the nature of the domains (hard versus soft phase) and their spatial orientation, is presented.

Much of the initial, analytical work [9] on the interacting Ostwald ripening problem focused on the equilibrium shapes and transformations of ordered domains. In many of these calculations, the geometrical shapes of the domains were fixed due to the numerical and analytical complexity of the problem. However, as pointed out [10,11], such geometrical constraints are simply not valid when a large number of elastically interacting domains are involved, and this can lead to artificial dynamics. Simulation approaches have, for the most part, been free from this problem, and include Monte Carlo studies [12], phase-field approaches [10,11,13,14], and the numerical integration of a set of interface equations [15]. While these different studies have all been invaluable in elucidating different aspects of the elastic Ostwald ripening problem, they have been confined to either 2D, or to 3D systems with only a small number of domains. At present, it is simply not clear which of the different results carry over from the case 2D into the experimentally more realistic 3D case. In addition, the lack of 3D theoretical data for the different morphological measures presently precludes any meaningful comparison with existing experimental data, and thereby underscores the need for 3D work.

To investigate phase separation with elasticity, we used a Langevin approach, extending a model introduced by Cahn [16] and Onuki [10]. The model assumes coherency at the interfaces (i.e., no dislocations), anisotropic elasticity, and differences between the elastic constants of the matrix and the precipitates. It is expressed in terms of the order parameter field $\psi(\vec{\mathbf{x}},t)$, the displacement fields $\mathbf{u}(\vec{\mathbf{x}},t)$, and the elastic strain tensor $\mu_{ij}=1/2(\partial u_i/\partial x_j+\partial u_j/\partial x_i)$. The most important parameters are the set of dimensionless elastic coefficients C_{ij}, which are related to the unscaled coefficients C_{ij}^* by $C_{ij}=C_{ij}^*\ell/\sigma$, where ℓ is a characteristic system length (e.g., the size of domains upon nucleation), and σ is the interfacial surface tension. These inhomogeneous elastic coefficients vary linearly with the order parameter, so that $C_{ij}=C_{ij}^o+C_{ij}'\tilde{\psi}$, with $\tilde{\psi}=\psi-\psi_o$ and ψ_o denoting the average value of the order parameter.

The free energy functional of the model is

$$F[\psi]=\int d\mathbf{x}[\tfrac{1}{2}|\nabla\psi|^2+f(\psi)+\alpha\psi\boldsymbol{\nabla}\cdot\mathbf{u}+f_{el}(\mu)], \quad (1)$$

where $f(\psi)=-\frac{1}{2}\psi^2+\frac{1}{4}\psi^4$ is the local free energy, α is a coupling constant, and f_{el} is the cubic elastic free energy:

$$f_{el}=\frac{\kappa}{2}(\boldsymbol{\nabla}\cdot\mathbf{u})^2+C_{44}\sum_{i\neq j}\mu_{ij}^2+M\sum_i\left(\mu_{ii}-\frac{1}{d}\boldsymbol{\nabla}\cdot\mathbf{u}\right)^2, \quad (2)$$

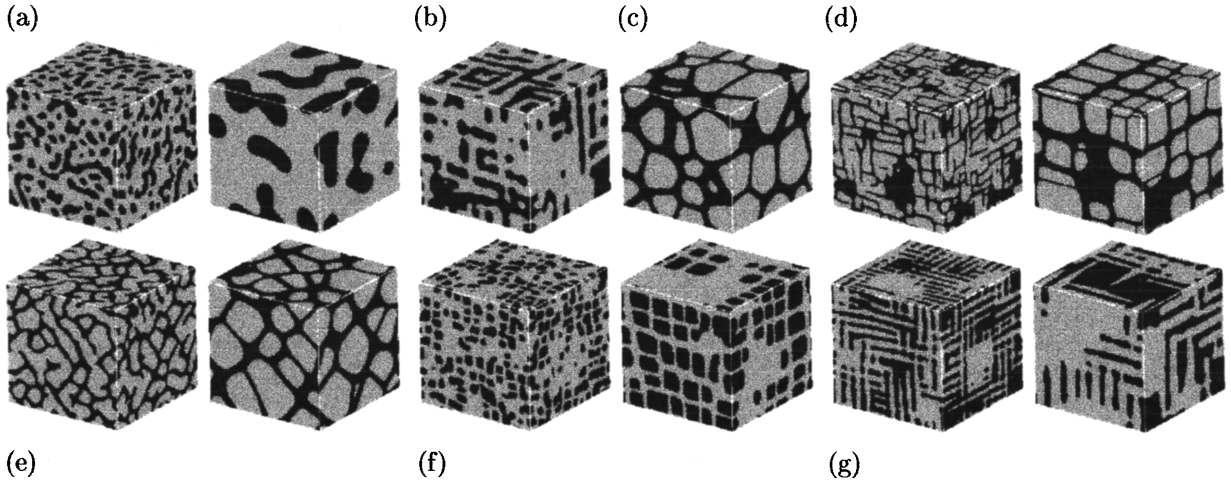

FIG. 1. Sample configurations at $\psi_o=0.3$ for different values of (g_1,g_2,τ_o). (a) (0,0,0), model B system at times $t=200$ and $t=10\,000$ (left and right, respectively); (b) (0, 0, 0.25) at $t=5000$; (c) (0.5, 0.5, 0) at $t=5200$; (d) (0.5, 0.5, 0.25) at $t=100$ and $t=10\,000$; (e) $(0.5, 0.5, -0.19)$ at $t=200$ and $t=4000$; (f) $(0.1, -0.4, 0.125)$ at $t=200$, and $t=2500$; and (g) $(0.24, -0.08, 0.7)$ at $t=200$ and $t=1000$. Note that the majority phase $\psi=+1$ is shown in gray, while the minority phase $\psi=-1$ is in black.

with compressibility modulus $\kappa=[C_{11}+(d-1)C_{12}]/d$, shear moduli C_{44}, and $M=(C_{11}-C_{12})/2$, which correspond to (100)[010] and (110)$[1\bar{1}0]$ shears, respectively. Invoking mechanical stability yields a set of equations relating ψ and **u**, which may then be used to eliminate **u** from the free energy. To first order in the coefficients C'_{ij} and anisotropy $B_o=(C^o_{11}-C^o_{12}-2C^o_{44})/C^o_{44}$, the elastic terms of the free energy combine to form an effective long-range free energy f_{lr}:

$$f_{lr}=\mu_d\sum_{i\neq j}\left(\frac{\partial^2 W}{\partial x_i\partial x_j}\right)^2+\mu_c\sum_i\left(\frac{\partial^2 W}{\partial x_i^2}-\frac{1}{d}\nabla^2 W\right)^2, \quad (3)$$

where $\mu_d=g_1\tilde{\psi}+\tau_o$, $\mu_c=g_2\tilde{\psi}$ represent (110)$[1\bar{1}0]$ and (100)[100] shears, respectively, and W represents a potential function defined via $\nabla^2 W=\tilde{\psi}$. In this model, the elastic misfit is proportional to $\delta=-\alpha/(C^o_{12}+2C^o_{44})$, so that the two coupling constants of f_{lr} are defined in terms of $g_1=C'_{44}\delta^2$, $g_2=(C'_{11}-C'_{12})\delta^2/2$, and $\tau_0=-C^o_{44}B^o\delta^2/2$. The g terms originate in the differences between the elastic coefficients of the matrix and the precipitates, while τ_o is independent of any such differences [17].

With the free energy functional expressed entirely in terms of ψ, the time evolution of the order parameter, following a quench, is given by the Langevin equation:

$$\partial\psi/\partial t=\nabla^2(\delta F/\delta\psi), \quad (4)$$

where we have neglected thermal noise. This equation was discretized ($\Delta x=1.7$) and integrated in time using Euler's method (time step $\Delta t=0.05$). Fast-Fourier transforms were used in the computation of W. Periodic boundary conditions for $(128)^3$ lattices were used, and systems of size $(64)^3$ were run to study finite size effects.

We have explored phase separation as a function of the off-criticality ψ_o and the parameters (g_1,g_2,τ_o). These parameters can either cooperate or compete with each other, and ultimately determine the final shape, orientation, spatial distribution and the elastically hard/soft nature of the precipitates. We find that in both two dimensions and three dimensions, the domain morphology is primarily determined by a single criterion: The domain structure formed is such that the matrix separating the precipitates holds most of the elastic distortions. For the model considered here, this is determined through a selection of the numerically *smallest* effective shear coefficient, i.e., the minimum value of either μ_d or μ_c *in the matrix*. The argument for this is as follows. Consider a two-phase inhomogeneous system with cubic symmetry. The system is characterized by *four* possible effective shear moduli, i.e., μ_c and μ_d with $\tilde{\psi}=\pm 1$ either for the matrix or precipitates, respectively. Roughly speaking, a minimization of the free energy (3) requires that the elastically ''hard'' phase deform less than the ''soft'' phase. Thus, a single hard domain in a soft matrix remains spherical or cuboidal, while a soft precipitate becomes needlelike or disklike. During spinodal decomposition, it is energetically favorable for the system to form compact, bounded domains with minimal elastic energy, so that most of the elastic energy is stored in the relatively deformable, percolating matrix. As phase separation continues, the matrix aligns itself and reshapes the domains so as to reduce the elastic energy. As an example, consider the following. The possible values for the shear moduli in (3) are $\mu_d=g_1+\tau_o$, $\mu_c=g_2$, for $\tilde{\psi}=+1$, and $\mu_d=-g_1+\tau_o$, $\mu_c=-g_2$, for $\tilde{\psi}=-1$. Suppose μ_d with $\tilde{\psi}=+1$ has the smallest numerical value. Then, for this particular quench, the matrix will be represented by $\tilde{\psi}=+1$, the precipitates by $\tilde{\psi}=-1$, and the system orients itself along the diagonal directions.

Consider different (g_1,g_2,τ_o) quenches at constant $\psi_o=0.3$, shown in Fig. 1. The domain morphologies are all to be compared to Fig. 1(a) with (0,0,0), i.e., no elastic effects. In this case, percolating domains following standard LSW dynamics are formed. The addition of *homogeneous* elastic fields via $(0,0,b)$ modifies the orientation of the domains. Highly anisotropic domains oriented in the cubic (diagonal) directions for $b>0$ ($b<0$) form, which percolate even at low volume fractions [Fig. 1(b)]. In the presence of *inhomo-*

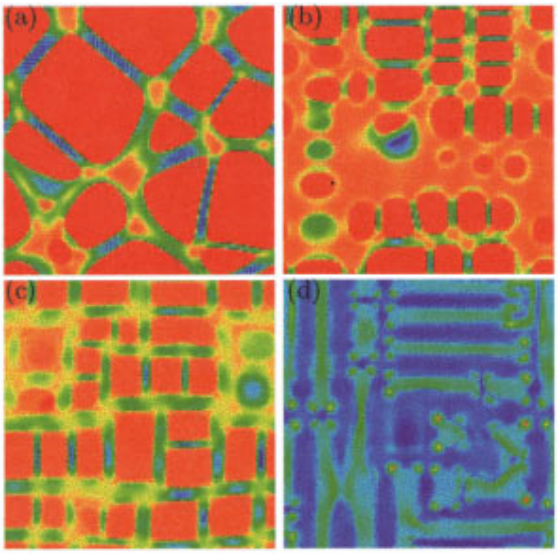

FIG. 2. (Color) Contour plots of elastic contribution to the chemical potential for cuts through sample configurations. Here, color indicates *relative* levels of the dimensionless potential running from deep red (high values) to deep blue (low values). Parameters (g_1, g_2, τ_o) are (a) (1.0, 1.0, 0), precipitate in the majority; (b) $(0.5, 0.5, -0.19)$, precipitate in the minority; (c) $(0.1, -0.4, 0.125)$, competing elastic effects; and (d) $(0.24, -0.08, 0.7)$, τ_o dominating.

geneous elastic constants, isolated precipitates always form; A $(0,b,0)$ $[(b,0,0)]$ quench gives domains with interfaces oriented along the cubic (diagonal) directions, while $(b,b,0)$ [Fig. 1(c)] gives *hard*, isotropic precipitates, because both types of shears are represented in equal proportions. While initially rounded, these precipitates develop flat faces at random orientations due to the proximity of other domains—this effect is most pronounced when the precipitates belong to the majority phase, as shown. The addition of homogeneous anisotropic effects influences the orientation of the precipitates in a predictable fashion [Figs. 1(d) and 1(e)]. Figures 1(f) and 1(g) illustrate different cases of elastic competition; the parameters are such that the precipitate formed is *soft* with respect to g_1 [18]. Particularly note the rafting of soft domains in Fig. 1(g), induced by the high anisotropy. We have also explored quenches for which the minimum values of μ_c and μ_d have the same numerical value. In this case, the system is frustrated with respect to the orientation of the precipitates, and other variables, such as the value of ψ_o, play a role in determining the morphology. Also, systems for which the effective moduli are very close in value are characterized by long-lived transients and crossover effects [19].

Figure 2 shows sample contour plots of the elastic contribution to the chemical potential landscape. In general, domains represent regions of negligible deformation, while significant distortions are found within the matrix. The elastic energy associated with these deformations creates chemical potential barriers, which control the diffusional flow of material between the precipitates. Domains that are surrounded by high barriers find it difficult to exchange material with other precipitates and, therefore, cease to grow. We now consider some generic situations. For the case of elastically hard, majority precipitates, the formed barriers are relatively large

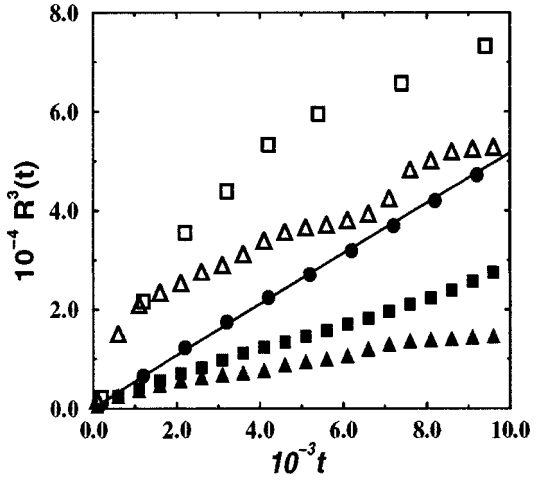

FIG. 3. $R(t)^3$ vs time for some three-dimensional systems. Filled circles, data for straight model B (five independent runs); open (filled) squares, $\psi_o = 0.3(-0.3)$ with parameters (0.5, 0.5, 0.125); and open (filled) triangles, $\psi_o = 0.3(-0.3)$ with (1.0, 1.0, 0.125). These data are averaged over only two independent runs.

(about 2.2–2.5) [Fig. 2(a)]. In contrast, when the domains form the minority phase [Fig. 2(b)], the barriers are considerably lower (about 1.0–1.5). Apparently, the elastic energy is spread out over the larger volume of the matrix. We note that there are no barriers when the precipitates (matrix) are soft (hard), reflecting the elastic competition [Fig. 2(c)]. In fact, in this case, the precipitates represent regions of high chemical potential (difference of 0.8), and material is readily exchanged between the domains. In the case of Fig. 2(d), the system is dominated by the homogeneous τ_o term giving a very gradual variation in the energy (difference of 0.23). The spatial ordering of domains is particularly evident in Figs. 2(b) and 2(c).

The time evolution of $R(t)$, defined as the first zero of the pair-correlation function, for sample quenches, is shown in Fig. 3. In the absence of *inhomogeneous* elastic fields, the growth exponent is consistent with $n = 1/3$, characteristic of LSW dynamics. For elastically *inhomogeneous* systems, growth may roughly be divided into an early and a late-time regime. If the majority phase forms the precipitates, the early-time growth is accelerated with respect to model B. This increased initial growth rate appears to be associated with rapid reshaping and coalescence of the precipitates. Spatial ordering of the domains then takes place as the system crosses over to the late-stage regime, which is characterized by a slowing down of the growth. Increasing the value of the $g's$ decreases the onset time for the late stages. For low volume fractions, growth appears to be consistent with $n = 1/3$, but with lower rates of coarsening. In this case, no coalescence was observed, and in contrast to the 2D case, there is no freezing of the domain structure. These results may be understood in terms of the elastic barriers surrounding the domains. Whenever these barriers are low, growth rates are similar to LSW; when they are high, the coarsening rates are considerably reduced with numerical values of the $g's$ determining the onset time.

In summary, we have investigated phase separation in a model binary alloy system incorporating elastic effects with

3D Langevin simulations. The elastic effects of the model result from a dilational misfit and from inhomogeneities in the elastic constants. Following a quench, the system evolves in such a way as to minimize both its interfacial and elastic free energy. The latter is achieved by storing most of elastic energy in the matrix between the precipitates which, in turn, determines the domain morphology as predicted from a selection rule. Different coarsening regimes have been observed, which correlate with the chemical potential barriers in the matrix. As is evident from the figures, the systems also display transient shape transformations, spatial ordering, and rafting of the domains. In addition, we have observed evidence for dynamic scaling of the structure factor, and have been able to induce reverse coarsening for selected domain configurations. These results, along with other measures of the domain morphology will be presented in a future publication [19].

This work was supported by the NSF under Grant Nos. DMR-95000858, DOWRE-9870464, and PB96-1120 from DGICyT, Spain. We also thank the North Carolina Supercomputing Center for significant Cray T90 support.

[1] I. M. Lifshitz and V. V. Slyozov, J. Chem. Solids **19**, 35 (1961); C. Wagner, Z. Elektrochem. **65**, 581 (1961).

[2] A. G. Khatchaturyan, *Theory of Structural Transformations in Solids* (Wiley, New York, 1983).

[3] A. J. Ardell, R. B. Nicholson, and J. D. Eshelby, Acta Metall. **14**, 1295 (1966); A. Maheshwari and A. J. Ardell, Scr. Metall. Mater. **26**, 347 (1992); Phys. Rev. Lett. **70**, 2305 (1993); M. Meshkimpour and A. J. Ardell, Mater. Sci. Eng., A **185**, 153 (1994); J. Wimmel and A. J. Ardell, *ibid.* **183**, 169 (1994); A. B. Kamora, A. J. Ardell, and C. N. Wagner, Metall. Mater. Trans. A **27A**, 2888 (1996); J.-H. Cho and A. J. Ardell, Acta Mater. **45**, 1399 (1997).

[4] O. Paris, M. Faehrmann, and P. Fratzl, Phys. Rev. Lett. **75**, 3458 (1995).

[5] T. Miyasaki, K. Nakamara, and H. Mori, J. Mater. Sci. **14**, 1927 (1979); W. Hein, Acta Metall. **37**, 2145 (1989).

[6] H. Calderon and G. Kostorz, Mater. Res. Soc. Symp. Proc. **166**, 210 (1990); H. A. Calderon, G. Kostorz, Y. Y. Qu, H. J. Dorontes, J. J. Cruz, and J. G. Cobanas-Moreno, Mater. Sci. Eng., A **238**, 13 (1997).

[7] A. Ges, O. Fornaro, and H. Palacio, J. Mater. Sci. **32**, 3689 (1997).

[8] P. Fratzl, F. Langmayr, G. Vogl, and W. Miekeley, Acta Metall. Mater. **39**, 753 (1991); F. Langmayr, P. Fratzl, G. Vogl, and W. Miekeley, Phys. Rev. B **49**, 11 759 (1994).

[9] J. D. Eshelby, Prog. Solid. Mech. **2**, 89 (1961); J. K. Lee, D. M. Barnett and H. I. Aaronson, Metall. Trans. A **8**, 963 (1977); W. C. Johnson and J. W. Cahn, Acta Metall. **23**, 1839 (1984); W. C. Johnson and P. W. Voorhees, J. Appl. Phys. **61**, 1610 (1987); I. M. Kaganov and A. L. Roitburd, Zh. Eksp. Teor. Fiz. **94**, 156 (1988) [Sov. Phys. JETP **67**, 1173 (1988)]; A. G. Khatchaturyan, S. V. Semenovskaya, and J. W. Morris, Acta Metall. **36**, 1563 (1988); W. C. Johnson, M. B. Berkenpas, and D. E. Laughlin, *ibid.* **36**, 3149 (1988); K. Kawasaki and Y. Enomoto, Physica A **150**, 463 (1988); Y. Enomoto and K. Kawasaki, Acta Metall. **37**, 1349 (1989); T. Miyazaki and M. Doi, Mater. Sci. Eng., A **110**, 175 (1989).

[10] A. Onuki, J. Phys. Soc. Jpn. **58**, 3065 (1989); **58**, 3069 (1989); H. Nishimori and A. Onuki, Phys. Rev. B **42**, 980 (1990); J. Phys. Soc. Jpn. **60**, 1208 (1991); A. Onuki and H. Nishimori, *ibid.* **60**, 1 (1991); Phys. Rev. B **43**, 13 649 (1991).

[11] M. E. Thompson, C. S. Su, and P. W. Voorhees, Acta Metall. Mater. **42**, 2107 (1994).

[12] J. Gayda and D. J. Srolowitz, Acta Metall. **37**, 641 (1989); J. K. Lee, Scr. Metall. Mater. **32**, 559 (1995); P. Fratzl and O. Penrose, Acta Metall. Mater. **43**, 2921 (1995); C. A. Laberge, P. Fratzl, and J. Lebowitz, Phys. Rev. Lett. **75**, 4448 (1995).

[13] Y. Wang, L.-Q. Chen, and A. G. Khatchaturyan, Scr. Metall. Mater. **25**, 1387 (1991); **25**, 1969 (1991); Acta Metall. Mater. **41**, 279 (1993).

[14] C. Sagui, A. M. Somoza, and R. C. Desai, Phys. Rev. E **50**, 4865 (1994).

[15] P. W. Voorhees, G. B. McFadden, and W. C. Johnson, Acta Metall. Mater. **40**, 2979 (1992); C. H. Su and P. W. Voorhees, Acta Mater. **44**, 1987 (1996); **44**, 2001 (1996).

[16] J. W. Cahn, Acta Metall. **9**, 795 (1961); **10**, 179 (1962).

[17] Note that Ref. [10] only treats the special case $g_1 = g_2$.

[18] This resolves a contradiction between previous theories and experiments. For example, Ref. [10] predicts that formed precipitates will always be elastically hard. Here we see that competition between different elastic energy terms can lead to the formation of soft precipitates with respect to one of the shear moduli, in agreement with experimental observations.

[19] D. Orlikowski, C. Sagui, A. M. Somoza, and C. Roland (unpublished).